Energy 220 (2021) 119779

Contents lists available at ScienceDirect

Energy

journal homepage: www.elsevier.com/locate/energy

Performance analysis of a water ejector using Computational Fluid Dynamics (CFD) simulations and mathematical modeling

Victor Jorge de Oliveira Marum [a, *], Lívia Bueno Reis [a], Felipe Silva Maffei [b], Shahin Ranjbarzadeh [b], Ivan Korkischko [c], Rafael dos Santos Gioria [a], Julio Romano Meneghini [b]

[a] Department of Mining and Petroleum Engineering, Escola Politécnica, Universidade de São Paulo, Santos, SP, 11013-560, Brazil
[b] Department of Mechanical Engineering, Escola Politécnica, Universidade de São Paulo, São Paulo, SP, 05508-010, Brazil
[c] CECCO, Nuclear and Energy Research Institute, IPEN, CNEN, São Paulo, SP, 05508-000, Brazil

ARTICLE INFO

Article history:
Received 30 November 2019
Received in revised form
3 October 2020
Accepted 4 January 2021
Available online 7 January 2021

Keywords:
Ejector
Efficiency
Mathematical modeling
Computational Fluid Dynamics (CFD)

ABSTRACT

A quasi-one-dimensional (1D) mathematical model coupled with Computational Fluid Dynamics (CFD) simulations of a water ejector is presented. Using data from CFD simulations, the mathematical model was used to calculate the friction loss coefficients of the ejector components, to predict its maximum efficiency point and to delimit its envelope of operation. The CFD approach was validated with experimental data and employed the finite element method to test the main turbulence models found in the literature (k-ε, k-ω and k-ω SST) for incompressible-flow ejectors. A set of operational conditions (OP) was tested and results show that the k-ω SST turbulence model is the most suitable to capture the ejector flow characteristics in all OP. In addition, for higher entrainment ratio (M) values, it was observed a possible correlation between how well the boundary layer can be solved and how the model is able to capture the ejector efficiency curve. Moreover, for lower M values, another possible correlation may be stated between how the turbulence model is able to capture the velocity profile.

1. Introduction

The rising of global energy demand is associated with industrial technological development coupled with the world population growth and people's pursuit of higher living standards. Many problems may arise with increasing of energy consumption, including emissions of greenhouse gases, acceleration of global warming and rising of electricity demand.

Creating new policies for energy recovery, designing mechanical machines with higher energy efficiency and replacing devices that require high external load may be good alternatives to reduce global energy demand. Over time, some compressors and pumps have been replaced by ejectors in energetic systems. Ejectors are mechanical devices composed basically of a nozzle, a suction chamber, a mixing section and a diffuser (Fig. 1). Its working principle is based on momentum transfer from a high-pressure flow (primary flow) to a low-pressure flow (secondary flow) [1], without requiring external work. The main advantages that make ejectors often employed in the industry are structure with no moving parts [2], absence of lubricants or bearings [3], reliability and low installation cost [4].

Ejectors have been proved to be effective devices and their applications are extended to several segments, including aeronautical engineering to increase the reliability of aircraft propulsion (e.g. Ref. [5]), in the petroleum industry for artificial lift and flow assurance (e.g. Ref. [6]), in thermal energy refrigeration systems (e.g. Ref. [7]), in desalination processes (e.g. Ref. [8]), and also for laser tomography procedures (e.g. Ref. [9]).

However, ejectors have low efficiency compared with other mechanical devices (i.e. pumps and compressors) and they are constructed to achieve the best performance at specific operational conditions [10]. For this reason, their geometry must be appropriately designed and optimization studies are strongly recommended.

To understand the complex nature of the flow inside ejectors, theoretical mathematical modeling may provide relevant information. Although the internal flow field of ejectors is three-dimensional, one-dimensional (1D) mathematical approaches can

* Corresponding author.
E-mail address: victormarum@usp.br (V. Jorge de Oliveira Marum).

https://doi.org/10.1016/j.energy.2021.119779
0360-5442/

Nomenclature

a	mixing-section-to-diffuser area ratio
A	cross-sectional area
C_P	pressure coefficient
K	friction loss coefficient
M	entrainment ratio
$\dot{m}$	mass flow rate
N	pressure recovery ratio
N_{ideal}	ideal pressure recovery ratio
NXP	the distance between the nozzle outlet and mixing section inlet
P	static/mean pressure
$\overline{P}$	total pressure
Q	flow rate
R	nozzle-to-mixing-section area ratio
u_i'	fluctuation of velocity at the x direction of flow
u_j'	fluctuation of velocity at the y direction of flow
u_t	turbulent dynamic viscosity
U_i	mean velocity at the x direction of flow
U_j	mean velocity at the y direction of flow
V	velocity

Greek symbols

η	efficiency
η_{ideal}	ideal efficiency
μ	dynamic viscosity
ρ	density
τ	shear stress

Subscripts

1	referred to the primary flow
2	referred to secondary flow
3	referred to mixing flow
D	referred to the diffuser
M	referred to the mixing section
N	referred to the nozzle
NO	referred to the nozzle outlet
S	referred to the suction chamber
W	referred to the inner wall area of the mixing section
$i,\ n,s,v,o,t,d$	ejector positions

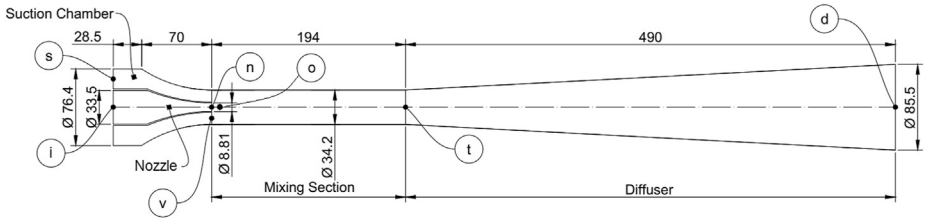

Fig. 1. Ejector geometry used for computational simulations. Dimensions in mm.

guide system operation, interpret experimental results, assist in system design and optimization [11], determine the ejector maximum efficiency points [12] and predict the ejector performance at critical and subcritical operation modes for compressible models [13].

Another solution for ejector modeling is the Computational Fluid Dynamics (CFD) technique, which provides a detailed description of the flow field inside ejectors by numerical solutions. CFD technique is proven to be an efficient tool to overcome some limitations of 1D mathematical approaches [14]. In recent years, CFD technique has been used to accurately investigate the influence of friction loss coefficients and ejector geometry on its performance [8,15,16], to study the flow distribution inside ejectors [17] and also to optimize the ejector geometrical parameters [18].

In this study, a quasi-1D mathematical approach (adapted from Ref. [19]) is employed to analyze the performance (or efficiency) of a water ejector using data from CFD simulations. In addition, a sequencing to estimate the friction loss coefficients of each ejector component (nozzle, suction chamber, mixing section and diffuser) is proposed based on [19]. The CFD approach was validated with experimental results [20] and the most suitable turbulence model was selected for further analysis.

2. Mathematical modeling

By applying conservation equations (mass, energy and momentum), a quasi-1D mathematical approach (adapted from Ref. [19]) was used to calculate the friction loss coefficients of each ejector component (nozzle, suction chamber, mixing section and diffuser), to predict the ejector maximum efficiency point (efficiency peak) and to determine the maximum theoretical efficiency that the ejector can reach (the envelope of operation).

The mathematical approach proposed by Ref. [19] assumes that pressures of the primary and secondary flows at the mixing section inlet have the same value (P_o). This assumption enables to express the ejector pressure recovery ratio (N) as a function independent of pressure data. It is very useful for situations where pressure and velocity data are unknown, and where only some geometrical parameters are known, as well as in experiments.

The adapted model described below considers that pressure of the primary flow at the nozzle outlet (P_n) and pressure of the secondary flow at the suction chamber outlet (P_v) have different values at the mixing section inlet, what in fact occurs in practice. This is the difference between both models. Considering different pressures at the mixing section inlet may provide more reliable results when pressure and velocity data are available and in results generated by computational simulations. This assumption considered in the adapted model significantly impacts the calculation of the friction loss coefficients.

2.1. Mathematical model development

The following assumptions were considered for the quasi-1D mathematical model formulation:

- Steady-state flow;
- Variations of gravitational potential energy between ejector inlets and outlet sections are neglected;
- Average values of pressure and velocity are considered in ejector sections;
- Both primary and secondary fluids are the same with incompressible flows (water is chosen as working fluid → $\rho = 998.2$ kg/m^3 = constant);
- The distance between nozzle outlet and mixing section inlet (*NXP*) is zero;
- The mixing section follows a constant-area configuration;
- Mixing flow inside the mixing section is one-dimensional (1D);
- Mixing between both primary and secondary flows is complete inside the mixing section.

This mathematical model [19] considers some dimensionless parameters, such as: entrainment ratio (M), nozzle-to-mixing-section area ratio (R) and mixing-section-to-diffuser area ratio (a). These parameters are defined as

$$M = \frac{Q_2}{Q_1} \tag{1}$$

$$R = \frac{A_{NO}}{A_M} \tag{2}$$

$$a = \frac{A_M}{A_D} \tag{3}$$

where Q_1 is the volumetric flow rate of the primary flow, Q_2 is the volumetric flow rate of the secondary flow, A_{NO} is the cross-sectional area of the nozzle outlet, A_M is the cross-sectional area of the mixing section and A_D is the cross-section area of the diffuser outlet.

Energy coupled with mass conservation equation for the nozzle (from position i to n in Fig. 1) can be expressed as

$$P_i + \rho_1 \frac{V_{1i}^2}{2} = P_n + \rho_1 \frac{V_{1n}^2}{2} + K_N \rho_1 \frac{V_{1n}^2}{2} \tag{4}$$

where P_i is the static pressure at the nozzle inlet, P_n is the static pressure at the nozzle outlet, ρ_1 is the density of the primary fluid, V_{1i} is the velocity of the primary flow at the nozzle inlet, V_{1n} is the velocity of the primary flow at the nozzle outlet and K_N is the friction loss coefficient of the nozzle.

Substituting the definition of the total pressure of the primary fluid at the nozzle inlet ($\overline{P}_i$), $\overline{P}_i = P_i + \rho_1 (V_{1i}^2/2)$, in equation (4), the nozzle equation becomes

$$\overline{P}_i = P_n + \rho_1 \frac{V_{1n}^2}{2}(1 + K_N) \tag{5}$$

For the suction chamber, the energy with mass conservation equation (from position s to v in Fig. 1) can be written as

$$P_s + \rho_2 \frac{V_{2s}^2}{2} = P_v + \rho_2 \frac{V_{2v}^2}{2} + K_S \rho_2 \frac{V_{2v}^2}{2} \tag{6}$$

where P_s is the static pressure at the suction chamber inlet, P_v is the static pressure at the suction chamber outlet, ρ_2 is the density of the secondary fluid, V_{2s} is the velocity of the secondary fluid at the suction chamber inlet, V_{2v} is the velocity of the secondary fluid at the suction chamber outlet and K_S is the friction loss coefficient of the suction chamber.

Substituting the total pressure at the suction chamber inlet ($\overline{P}_s$), $\overline{P}_s = P_s + \rho_2 (V_{2s}^2/2)$, in equation (6), the suction chamber equation becomes

$$\overline{P}_s = P_v + \rho_2 \frac{V_{2v}^2}{2}(1 + K_S) \tag{7}$$

Momentum coupled with mass conservation equation for the mixing section (from position o to t in Fig. 1) is

$$\left(\dot{m}_1 + \dot{m}_2\right) V_{3t} - \dot{m}_1 V_{1n} - \dot{m}_2 V_{2v} = (P_o - P_t) A_M - \tau A_W \tag{8}$$

where $\dot{m}_1$ is the mass flow rate of the primary flow, $\dot{m}_2$ is the mass flow rate of the secondary flow, V_{3t} is the velocity of the mixing flow at the mixing section outlet, P_o is the static pressure at the mixing section inlet, P_t is the static pressure at the mixing section outlet, τ is the shear stress and A_W is the inner wall area of the mixing section.

Dividing all terms in equation (8) by A_M, substituting the definitions of friction loss, $\tau(A_w/A_M) = K_M \rho_3 (V_{3t}^2/2)$, mass flow rate, $\dot{m} = \rho V A$, and R, it can be written as

$$P_o - P_t = [V_{1n} R \rho_1 + V_{2v}(1 - R)\rho_2] V_{3t} - V_{1n}^2 R \rho_1 - V_{2v}^2 (1 - R)\rho_2 + K_M \rho_3 \frac{V_{3t}^2}{2} \tag{9}$$

where K_M is the friction loss coefficient of the mixing section and ρ_3 is the density of the mixing flow.

Applying the energy and mass conservation equations in the diffuser (from position t to d in Fig. 1), it results in Ref. [19].

$$P_t + \rho_3 \frac{V_{3t}^2}{2} = P_d + \rho_3 \frac{V_{3d}^2}{2} + K_D \rho_3 \frac{(V_{3t} - V_{3d})^2}{2} \tag{10}$$

where P_d is the static pressure at the diffuser outlet, V_{3d} is the velocity of the mixing flow at the diffuser outlet and K_D is the friction loss coefficient of the diffuser.

Substituting the total pressure at the diffuser outlet ($\overline{P}_d$), $\overline{P}_d = P_d + \rho_3 (V_{3d}^2/2)$, in equation (10), the diffuser equation turns [19].

$$\overline{P}_d = P_t + \rho_3 \frac{V_{3t}^2}{2} - K_D \rho_3 \frac{(V_{3t} - V_{3d})^2}{2} \tag{11}$$

where P_d is the static pressure at the diffuser outlet, V_{3d} is the velocity of the mixing flow at the diffuser outlet and K_D is the friction loss coefficient of the diffuser.

Equations (5), (7), (9) and (11) can be applied for cases when both primary and secondary fluids are incompressible with different densities. For water ejectors, when both primary and secondary fluids are water ($\rho_1 = \rho_2 = \rho_3 = \rho$), these equations can be written, respectively, as

$$\overline{P}_i = P_n + \rho \frac{V_{1n}^2}{2}(1 + K_N) \tag{12}$$

$$\overline{P}_s = P_v + \rho \frac{V_{2v}^2}{2}(1 + K_S) \tag{13}$$

$$P_o - P_t = \rho \left\{ [V_{1n} R + V_{2v}(1 - R)] V_{3t} - V_{1n}^2 R - V_{2v}^2 (1 - R) + K_M \frac{V_{3t}^2}{2} \right\} \tag{14}$$

$$\overline{P}_d = P_t + \frac{\rho}{2} V_{3t}^2 \left[1 - K_D(a-1)^2\right] \tag{15}$$

Ejector pressure recovery ratio (N) is a dimensionless parameter of interest which is expressed in terms of total pressures at the nozzle inlet, suction chamber inlet and diffuser outlet. It can be defined as

$$N = \frac{\overline{P}_d - \overline{P}_s}{\overline{P}_i - \overline{P}_d} \tag{16}$$

Applying the very restrictive assumption used by Ref. [19], which considers that the static pressures at the nozzle outlet (P_n) and suction chamber outlet (P_v) have the same value at the mixing section inlet (P_o), N can be also expressed as

$$N = \frac{2R + \frac{2M^2R^2}{1-R} - \left[1 + K_M + (1-a)^2 K_D\right] R^2 (1+M)^2 - (1+K_S)\frac{M^2R^2}{(1-R)^2}}{1 + K_N - 2R - \frac{2M^2R^2}{1-R} + \left[1 + K_M + (1-a)^2 K_D\right] R^2 (1+M)^2} \tag{17}$$

Theoretical ideal pressure recovery ratio (N_{ideal}) equation is obtained by assuming all friction loss coefficients equal to zero in equation (17). Thus, it turns

$$N_{ideal} = \frac{2R + \frac{2M^2R^2}{1-R} - R^2(1+M)^2 - \frac{M^2R^2}{(1-R)^2}}{1 - 2R - \frac{2M^2R^2}{1-R} + R^2(1+M)^2} \tag{18}$$

Ejector efficiency (η) can be defined as the ratio of the energy transferred to the secondary flow to the energy available from the primary flow [21], and it can be written as

$$\eta = M \times N \tag{19}$$

Theoretical ideal efficiency (η_{ideal}), which represents the maximum efficiency that ejector can achieve (the envelope of operation), is defined as

$$\eta_{ideal} = M \times N_{ideal} \tag{20}$$

The friction loss coefficients of the nozzle (K_N), suction chamber (K_s), mixing section (K_M) and diffuser (K_D) were calculated fitting CFD data to the equations (12)–(15), respectively, with constant ρ = 998.2 kg/m^3, $R = 0.066$, $a = 0.16$ and average P and V data from CFD simulations as input parameters.

3. Computational method

The geometry used in the simulations was built based on the ejector model used by Ref. [20]. From the original ejector, some simplifying assumptions were introduced. To guarantee that these simplifications do not produce considerable errors in the results, several simulations were carried out using the k-ε model and no significant variation in the results was pointed out. The final geometry is depicted in Fig. 1. Its 2D axisymmetric property was used in the simulations and the error related to this simplification was considered negligible [22].

CFD simulations were carried out using the commercial software COMSOL Multiphysics®, which employs a finite element discretization scheme. Because of the flow complexity, Reynolds-Averaged Navier Stokes (RANS) equations were employed as a suitable way to achieve a balanced result between accuracy and computational cost. The simulations were performed based on the following assumptions: i) Newtonian fluid; ii) Boussinesq assumption for the Reynolds stresses; iii) Adiabatic; iv) Incompressible flow; v) Steady-state flow; vi) Constant viscosity; vii) Negligible body forces; and viii) Both fluids are water at 26.7 °C. Thus, the solved equations for averaged mass and momentum conservation are written, respectively, as

$$\frac{\partial(\rho U_j)}{\partial x_j} = 0 \tag{21}$$

$$\frac{\partial}{\partial x_j}(U_i U_j) = -\frac{\partial P}{\partial x_i} + \frac{\partial}{\partial x_j}\left(\tau_{ij} - \rho\overline{u_i' u_j'}\right) \tag{22}$$

where ρ is the density, U_i is the mean velocity at the x-direction of flow, U_j is the mean velocity at y-direction of flow, P is the mean pressure, u_i' is the fluctuation of velocity in x-direction and u_j' is the fluctuation of velocity in y-direction.

Reynolds stress tensor and shear stress were calculated by equations (23) and (24), respectively:

$$-\rho\overline{u_i' u_j'} = u_t\left(\frac{\partial U_i}{\partial x_j} + \frac{\partial U_j}{\partial x_i}\right) \tag{23}$$

$$\tau_{ij} = \mu\left(\frac{\partial U_i}{\partial x_j} + \frac{\partial U_j}{\partial x_i}\right) \tag{24}$$

where μ is the dynamic viscosity and u_t is the turbulent dynamic viscosity.

Three turbulence models were tested: k-ε [23], k-ω [24] and k-ω SST [25], using their respective standard closure constraints [26]. The wall treatment *Wall function* was set to the k-ε model and *automatic* to k-ω and k-ω SST models. The automatic wall treatment was selected because it improves the robustness of the model, switching between the *low-Reynolds* and regular wall functions, depending on the flow near the wall [26].

The boundary conditions used for setting up the computational model are summarized in Table 1, where U_0 is the normal velocity, L_t is the turbulence scale (equal to $0.007 \cdot L$) and I_t is the turbulence intensity (equal to 0.05). The iterative method for nonlinear equation used in simulations was assumed converged when the relative error is equal or less than 0.001 for all quantities.

The meshes used in this study were unstructured, composed by triangular and quadrilateral elements. To control the error from discretization, the initial mesh (automatically generated) was refined using an adaptive technique. This approach uses results from the previous mesh to improve the mesh quality in the region of the highest gradients. This way, the elements are more efficiently refined if compared with a situation where the number of elements is randomly increased. Four refinement steps were applied for each simulation conducted in this study, generating one mesh for each M and turbulence model. To verify the convergence of the mesh generated by the adaptive scheme, the root mean squared error (RMSE) was plotted as a function of the number of elements that composes the discretized domain. The RMSE was calculated between simulated and experimental data [20] of the pressure coefficient (C_P) at the ejector wall for $M = 3.56$. Summation of RMSE ran on the 18 pressure taps located in the same positions of the experiment conducted by Ref. [20]. Figs. 2, 3 and 4 show the convergence study of the meshes generated by the scheme for the k-ε, k-ω and k-ω SST turbulence models, respectively.

The k-ε (Fig. 2) and k-ω (Fig. 3) turbulence models were the most affected by the adaptive iterations, while the k-ω SST (Fig. 4) model presents a slight variation in the RMSE values. Nevertheless, in all models it is observed the mesh adaption in the jet region (where a higher velocity gradient is presented) and the difference between each mesh emphasizes the different interpretation of the models in

Table 1
Values and properties of boundary conditions applied at the model.

Boundary	Mean field Value/Feature	Turbulent Value/Feature
Nozzle inlet (primary inlet)	Normal velocity equals to 2.0 m/s (1.77×10^{-3} m^3/s)	$k = \frac{3}{2}(U_0 I_t)^2$
Suction chamber inlet (secondary inlet)	Normal velocity (varies with M)	$\varepsilon = C_\mu^{3/4}\frac{k^{3/2}}{L_t}$
Diffuser outlet	Relative pressure equals to zero	$\partial_i k \cdot n_i = 0$ $\partial_i \varepsilon \cdot n_i = 0$
Wall	No slip conditions	wall function (smooth wall)

the prediction of these structures.

In all three convergence studies, the convergence could be reached with only three adaptive steps (fourth point) instead of four steps, since the difference between the RMSE values obtained in the last two step (fourth and fifth points) is very small. However, as the computational time did not increase significantly from the third to the fifth point, the four iterative steps remained.

The CFD simulations were validated by comparing the ejector efficiency curve, the pressure coefficient (C_P) distribution and the total pressure profiles generated by computational simulations with the experimental results from Ref. [20].

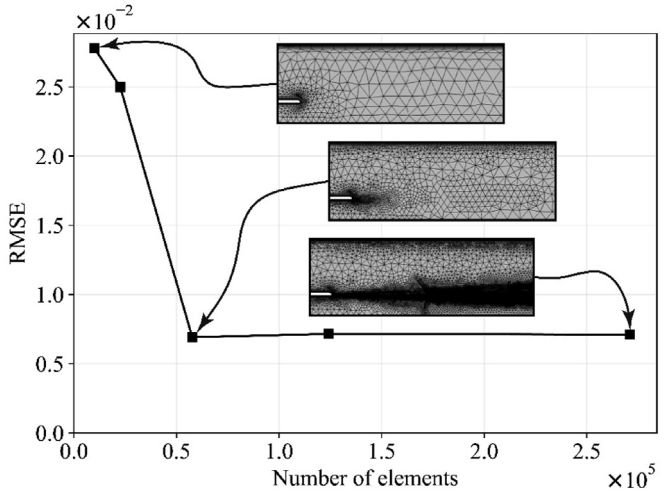

Fig. 2. Mesh convergence study for the k-ε turbulence model. The meshes depicted correspond to some of the refinement steps.

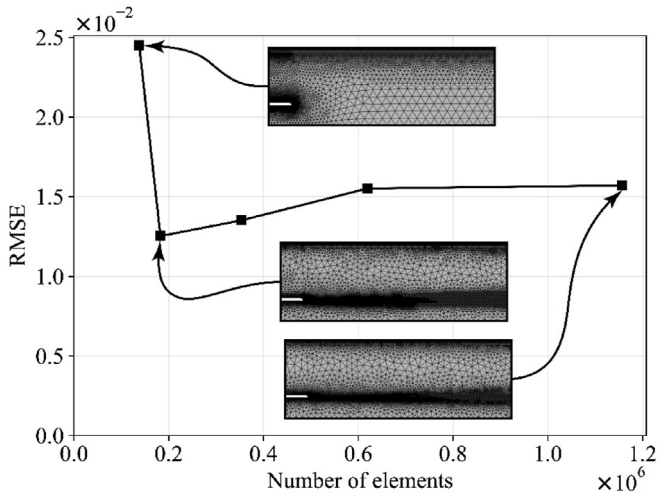

Fig. 3. Mesh convergence study for the k-ω turbulence model. The meshes depicted correspond to some of the refinement steps.

4. Results

4.1. Validation of the CFD simulations

The comparison between the k-ε, k-ω and k-ω SST turbulence models and the experimental data from Ref. [20] is presented in Fig. 5. Different values of P and V are given as results by CFD simulations for specific entrainment ratio M (i.e ratio between the secondary and primary flow rates) values. P and V data at the ejector cross-sectional regions were obtained for nine different M values (1.20, 1.74, 2.48, 3.04, 3.56, 4.02, 4.39, 4.61, 5.15). The efficiency curves for the three turbulence models were plotted using equation (18) with simulation data obtained for each corresponding M.

Fig. 5 shows that the k-ε and k-ω SST turbulence models are in good agreement with experimental data [20] up to $M = 3.56$. On the other hand, for values of M higher than the maximum efficiency point ($M = 4.02$), k-ε and k-ω SST have overestimated the ejector efficiency. The k-ω SST was the only model capable of predicting the peak-efficiency operational condition ($M = 4.02$) and it has also presented the best agreement with experimental data [20] for the highest entrainment ratio value ($M = 5.15$), while k-ω has proven to be unsatisfactory for almost all M values in this study. The current result is in agreement with the literature [27], which encountered that the k-ω SST turbulence model is adequate for numerical simulations of ejectors.

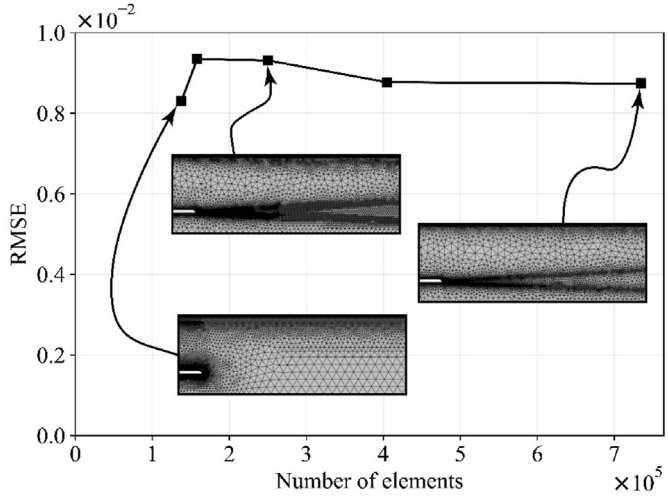

Fig. 4. Mesh convergence study for the k-ω SST turbulence model. The meshes depicted correspond to some of the refinement steps.

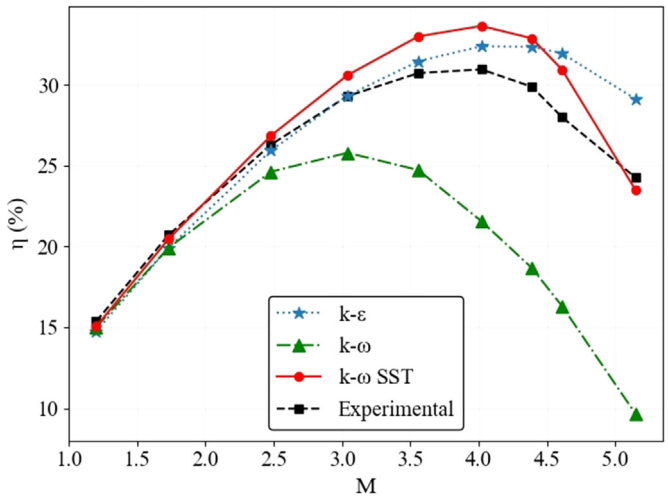

Fig. 5. Ejector efficiency (η) as a function of the entrainment ratio (M) for k-ε, k-ω and k-ω SST turbulence models in comparison with experimental data from Ref. [20].

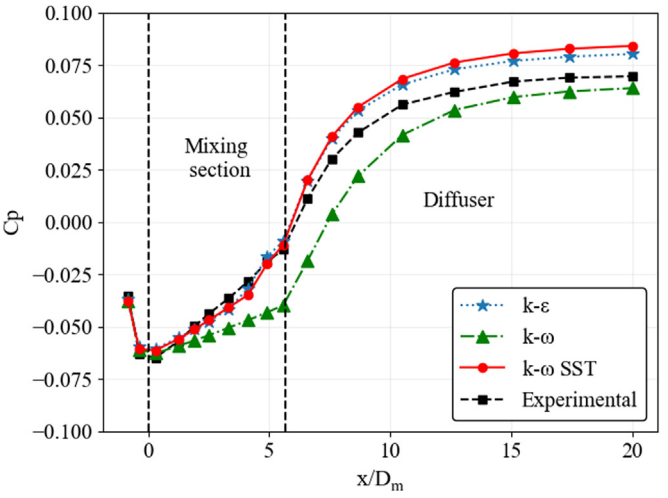

Fig. 6. Distribution of the pressure coefficient (C_P) as a function of the dimensionless position calculated by the ratio between the distance of pressure tap from the nozzle (x) and the diameter of the mixing section (D_M), plotted for k-ε, k-ω and k-ω SST turbulence models, and experimental data from Ref. [20].

Fig. 6 shows the distribution of the pressure coefficient (C_P) on the ejector wall as a function of a dimensionless position calculated by the ratio between the distance of pressure tap from the nozzle (x) and the diameter of the mixing section (D_M). The k-ε and k-ω SST models could accurately predict the static pressure distribution and recovery (referred to the mixing process [20]) up to the mixing section outlet position. In the diffuser, both k-ε and k-ω SST models overestimated the static pressure recovery from the flow deceleration, while the k-ω could not accurately predict the static pressure in all ejector length investigated. Overprediction of the turbulence model in the ejector performance is probably related to the static pressure overestimation. This behavior may be associated with the absence of information about the roughness of the ejector wall used in the experiment. Thus, the ejector investigated through CFD simulations (which employ the smooth wall assumption [28]) dissipates less energy than the ejector tested in the experiments.

Furthermore, to closely investigate the turbulence models accuracy in the jet structure prediction and boundary layer behavior, the total pressure profiles were plotted at three positions x/D_M (2.6, 4.8 and 10.4), the first two positions in the mixing section and the later in the diffuser, for $M = 3.56$ (Fig. 7), with corresponding experimental data [20]. And the average and minimum shear stresses in the mixing section and diffuser walls were plotted as a function of M in Fig. 8.

Fig. 7 allows a comparison of the capability of each turbulence model to predict the jet structure through the total pressure profile at different axial positions along the ejector. It is shown that k-ε and k-ω SST models presented the best agreement with experimental data, with k-ε showing slightly better results, whereas the k-ω model unsatisfactorily estimated the jet profile along all the axial positions investigated. Moreover, k-ε and k-ω SST models have overestimated the static pressure at the ejector wall in all cases.

Using the averaged shear stress at each flow condition (M) (Fig. 8), it was possible to compare the estimation of friction losses and the behavior of the boundary layer regarding its detachment by tracking the change of shear stress sign [29]. It is observed that the wall shear stress (WSS) predicted by the k-ε model presented the lowest value between the tested models, whereas the k-ω and k-ω SST models showed similar behavior in almost all points for M lower than 4. The exception was noticed at the last four operational points where the k-ω model showed a crescent behavior, whereas the k-ω SST stabilizes. This difference may be attributed to the significant difference between k-ω and k-ω SST models in predicting the jet structure (Fig. 7). Despite the differences in their values, no point of flow detachment was identified, i.e., no change in the signal of minimum shear stress was observed.

By comparing the distribution of total pressure profiles (Fig. 7) and the efficiency curve (Fig. 5), it can be inferred that the good agreement of the turbulence model with experimental data for lower M values is associated with this ability to correctly capture the velocity profiles. It occurs at these conditions because the mixing caused by the jet plays an essential role in the ejector performance [20]. As M increases, the effect of boundary layer (regarding to friction losses) starts playing an important role in the ejector performance [20], and all turbulence models diverge about the intensity of friction losses at this point (Fig. 8). k-ω SST points out higher averaged values of wall shear stresses for all M values, whereas k-ε presents lower stress values. Thus, it is possible to establish a correlation between the superior performance of the k-ω SST turbulence model and the ability to accurately evaluate the boundary layer. The k-ω model could not satisfactorily predict the mixing profile; therefore the boundary layer behavior was compromised.

4.2. Envelope curve and calculation of the friction loss coefficients

Using data from computational simulations (i.e., averaged pressure and velocity at the cross-sectional areas at positions i, n, s, v, o, t, d), constant $\rho = 998.2$ kg/m^3, $R = 0.066$ and $a = 0.16$, the friction loss coefficients of the nozzle (K_N), suction chamber (K_S), mixing section (K_M) and diffuser (K_D) were calculated fitting CFD data to equations (12)–(15), respectively, for each M mentioned before.

From equation (16) it is possible to calculate a corresponding N for each M and also the ejector efficiency curve using equation (19). The same procedure is employed to obtain the ideal efficiency curve (i.e. the envelope of operation), but considering equations (18) and (20).

The efficiency curves plotted with the calculated friction loss coefficients were obtained for each M. In the present study, the efficiency curve for $M = 1.20$ has presented the closest agreement (or lower RMSE) with the efficiency curve obtained from CFD data (k-ω SST), as shown in Table 2. The RMSE values were calculated

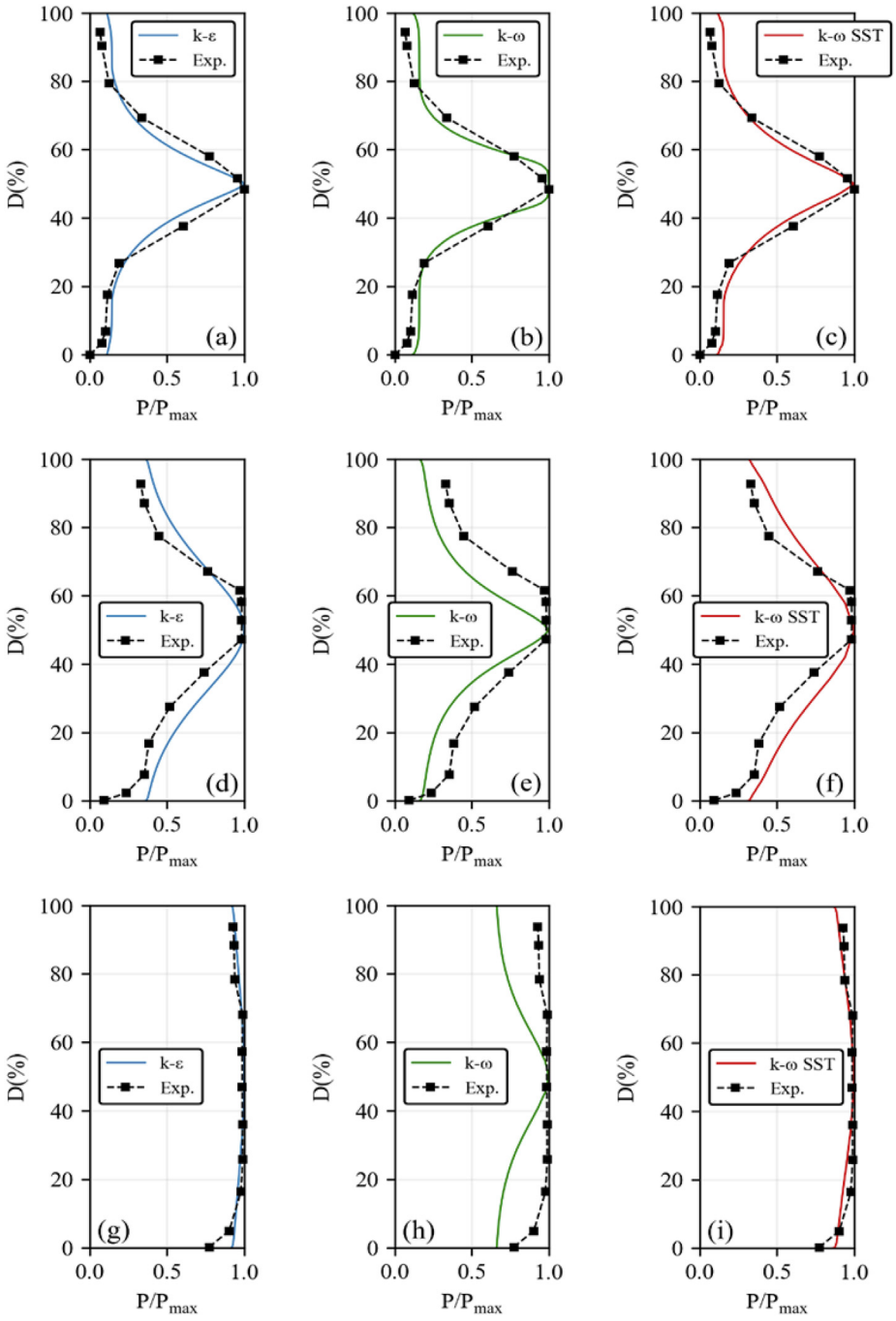

Fig. 7. Total pressure profiles. In the vertical axis, the position of the probe measured in percentage counted initially from the top wall of the ejector. In the horizontal axis, the total pressure (P) normalized by the maximum pressure value (P_{max}) measured. Dashed green lines correspond to experimental results (in the legend abbreviated by Exp.). From (a) to (c), profiles were taken at 2.6 x/D_M for each turbulence model. From (d) to (f), profiles were taken at 4.8 x/D_M for each turbulence model. From (g) to (i), profiles were taken at 10.4 x/D_M. Experimental data from Ref. [20].

between the efficiency obtained from CFD data and the efficiency modeled by the 1D model for each M. Thus, the friction loss coefficients estimated using $M = 1.20$ were selected for further analysis in this paper. The calculated friction loss coefficients for $M = 1.20$ were: $K_N = 0.0464$, $K_S = 0.1039$, $K_M = 0.0302$ and $K_N = 0.0792$.

The mathematical models, with the calculated friction loss coefficients, and the ideal efficiency (with no losses) are compared with CFD data in Fig. 9, where it presents: i) the efficiency curve plotted with calculated friction loss coefficients – *1D model ($M = 1.20$)*; ii) the efficiency curve generated from CFD simulation data – *CFD data (k-ω SST)*; and iii) the ejector theoretical maximum efficiency – *Ideal efficiency (envelope)*. The efficiency curve from simulation data was determined considering the turbulence model that showed the best agreement with experimental results (k-ω SST), as discussed in section 4.1.

From Fig. 9, it is observed that the efficiency curve plotted with the calculated friction loss coefficients (1D model) shows good agreement with simulation data, mainly for M values between 1.20 and 2.48, and the peak of both efficiency curves is coincident for

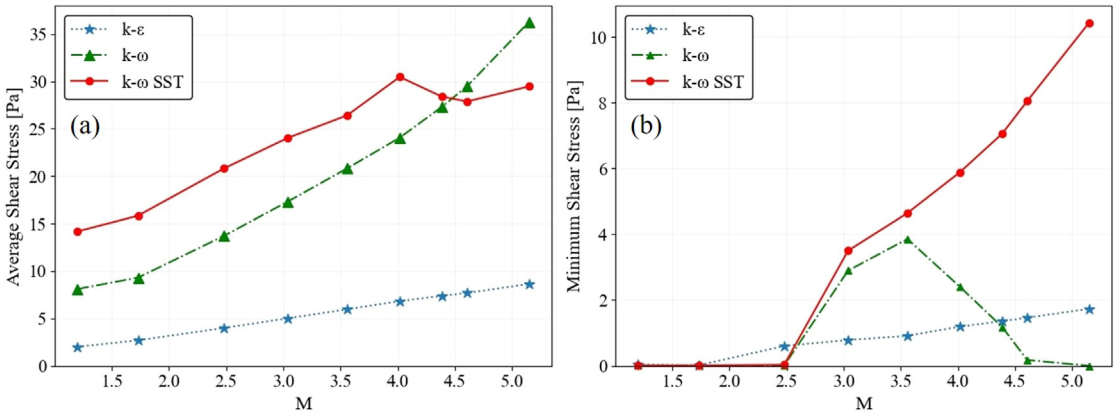

Fig. 8. Average Shear Stress (a) and Minimum Shear Stress (b) for each M at the mixing section and diffuser walls.

Table 2
Deviation of the efficiency curves plotted with the calculated friction loss coefficients from the efficiency curve obtained from CFD data, for each M.

M	1.20	1.74	2.48	3.04	3.56	4.02	4.39	4.61	5.15
RMSE (%)	0.32	0.59	1.38	2.26	3.15	3.74	3.79	3.97	7.18

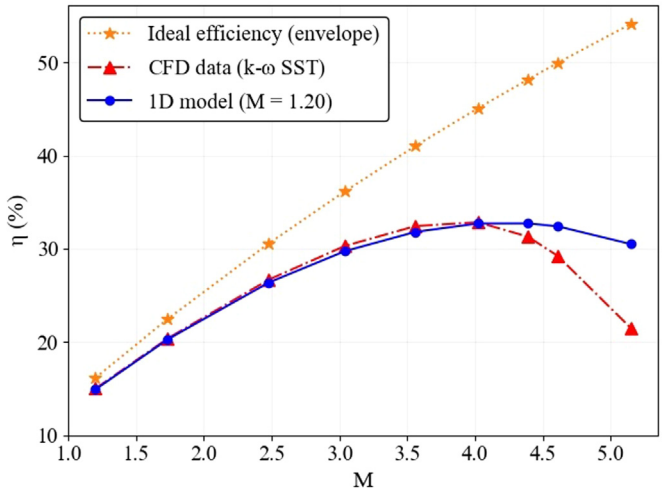

Fig. 9. Ejector efficiency plotted with the calculated friction loss coefficients by the 1D model, CFD data and the ideal efficiency (envelope of operation) for $M =$ 1.20.

$M = 4.02$. In addition, the ejector envelope of operation (ideal efficiency), estimated by the mathematical model, has accurately restricted the ejector's maximum efficiency for all operational conditions, considering that the simulation results should be below the theoretical maximum efficiency that the ejector can reach (envelope).

Deviations from the envelope of the efficiency curves plotted with the mathematical model and simulation results are presented in Fig. 10. In fluid-flow problems, the friction losses vary as a function of the squared-volumetric flow (Q^2). As the friction loss coefficients (K) were hypothetically kept constant with the M increment in this study to perform the theoretical analysis, the deviation of both 1D-model and CFD curves from the envelope (Fig. 10) shows quadratic behavior, that corroborates with the theoretical aspects.

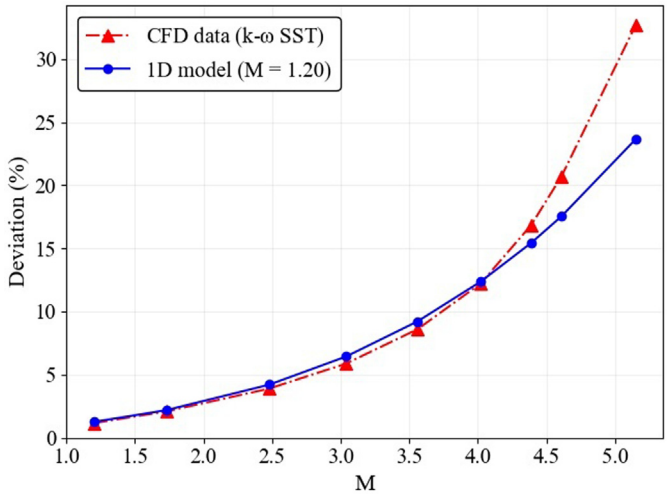

Fig. 10. Deviation from the envelope of the efficiency curves plotted with the 1D model and CFD data for $M = 1.20$.

5. Conclusions

The accuracy of a quasi-1D mathematical model to analyze the performance of an incompressible-flow ejector using data from CFD simulations was investigated. By comparing the k-ε, k-ω and k-ω SST turbulence models, the latter has proven to be the most suitable to capture the ejector's flow characteristics in all operational conditions, specially the peak-efficiency operational condition. The accuracy of the k-ω model was unsatisfactory.

The discussion of the results from the CFD simulations pointed out a possible correlation between how well the boundary layer can be solved and how the model is capable to capture the ejector efficiency curve for higher entrainment ratio (M) values, whereas at low M values the agreement between the simulated and experimental data is possible correlated with how well the turbulence models have captured the jet profiles.

After the comparison of the turbulence models, a modification to the mathematical model proposed by Ref. [19] was presented. It was shown that it can accurately delimit the ejector envelope of operation, predict its maximum efficiency point and calculate reliable values of the friction loss coefficients for each ejector component.

The original 1D model [19] is based on a very restrictive

assumptions regarding pressure distributions at the nozzle outlet (P_n), suction chamber outlet (P_v) and mixing section inlet (P_o) positions. In this study, it was shown through CFD simulations that the pressure profile at those positions have different values and it affects the calculation of the friction loss coefficients, as highlighted in the profiles plotted in Fig. 7. The quasi-1D model has proven to be a useful tool for preliminary analysis of project execution, because it is computationally cheaper than CFD simulations if properly calibrated using either CFD or experimental data when these are available.

Declaration of competing interest

The authors declare that they have no known competing financial interests or personal relationships that could have appeared to influence the work reported in this paper.

Acknowledgments

The authors gratefully acknowledge support from FAPESP and SHELL Brazil through the 'Research Centre for Gas Innovation – RCGI' (FAPESP Proc. 2014/50279-4), hosted by the University of Sao Paulo, and the support given by ANP (Brazil's National Oil, Natural Gas and Biofuels Agency) through the R&D levy regulation. L.B.R., I.K. and S.R. gratefully acknowledge support from FAPESP, Proc. 2019/05197-3, Proc. 2016/12397-0 and Proc. 2018/11474-7, respectively.

References

[1] Arbel A, Shklyar A, Hershgal D, Barak M, Sokolov M. Ejector irreversibility characteristics. J Fluid Eng 2003;125:121–9. https://doi.org/10.1115/1.1523067.
[2] Park BH, Lim JH, Yoon W. Fluid dynamics in starting and terminating transients of zero-secondary flow ejector. Int J Heat Fluid Flow 2008;29:327–39. https://doi.org/10.1016/j.ijheatfluidflow.2007.06.008.
[3] Little AB, Garimella S, DiPrete JP. Combined effects of fluid selection and flow condensation on ejector operation in an ejector-based chiller. Int J Refrig 2016;69:1–16. https://doi.org/10.1016/j.ijrefrig.2016.04.011.
[4] Shestopalov KO, Huang BJ, Petrenko VO, Volovyk OS. Investigation of an experimental ejector refrigeration machine operating with refrigerant R245fa at design and off-design working conditions. Part 1. Theoretical analysis. Int J Refrig 2015;55:201–11. https://doi.org/10.1016/j.ijrefrig.2015.01.016.
[5] Kracík J, Dvořák V. Experimental and numerical investigation of an air to air supersonic ejector for propulsion of a small supersonic wind tunnel. EPJ Web Conf 2015;92:1–5. https://doi.org/10.1051/epjconf/20159202038.
[6] Pedroso MC. Dinâmica dos fluidos computacional aplicada a ejetores. Universidade Estadual de Campinas; 2015.
[7] Besagni G, Mereu R, Inzoli F. Ejector refrigeration: a comprehensive review. Renew Sustain Energy Rev 2016;53:373–407. https://doi.org/10.1016/j.rser.2015.08.059.
[8] Wang C, Wang L, Wang X, Zhao H. Design and numerical investigation of an adaptive nozzle exit position ejector in multi-effect distillation desalination system. Energy 2017;140:673–81. https://doi.org/10.1016/j.energy.2017.08.104.
[9] Bouhanguel A, Desevaux P, Gavignet E. Flow visualization in supersonic ejectors using laser tomography techniques. Int J Refrig 2011;34:1633–40. https://doi.org/10.1016/j.ijrefrig.2010.08.017.
[10] Hamzaoui M, Nesreddine H, Aidoun Z, Balistrou M. Experimental study of a low grade heat driven ejector cooling system using the working fluid R245fa. Int J Refrig 2018;86:388–400. https://doi.org/10.1016/j.ijrefrig.2017.11.018.
[11] He S, Li Y, Wang RZ. Progress of mathematical modeling on ejectors. Renew Sustain Energy Rev 2009;13:1760–80. https://doi.org/10.1016/j.rser.2008.09.032.
[12] Antonio YM, Périlhon C, Descombes G, Chacoux C. Thermodynamic modelling of an ejector with compressible flow by a one-dimensional approach. Entropy 2012;14:599–613. https://doi.org/10.3390/e14040599.
[13] Chen W, Liu M, Chong D, Yan J, Little AB, Bartosiewicz Y. A 1D model to predict ejector performance at critical and sub-critical operational regimes. Int J Refrig 2013;36:1750–61. https://doi.org/10.1016/j.ijrefrig.2013.04.009.
[14] Lee MS, Lee H, Hwang Y, Radermacher R, Jeong HM. Optimization of two-phase R600a ejector geometries using a non-equilibrium CFD model. Appl Therm Eng 2016;109:272–82. https://doi.org/10.1016/j.applthermaleng.2016.08.078.
[15] Wu H, Liu Z, Han B, Li Y. Numerical investigation of the influences of mixing chamber geometries on steam ejector performance. Desalination 2014;353:15–20. https://doi.org/10.1016/j.desal.2014.09.002.
[16] Zhang H, Wang L, Jia L, Zhao H, Wang C. Influence investigation of friction on supersonic ejector performance. Int J Refrig 2018;85:229–39. https://doi.org/10.1016/j.ijrefrig.2017.09.028.
[17] Zhu Y, Jiang P. Experimental and numerical investigation of the effect of shock wave characteristics on the ejector performance. Int J Refrig 2014;40:31–42. https://doi.org/10.1016/j.ijrefrig.2013.11.008.
[18] Yadav RL, Patwardhan AW. Design aspects of ejectors: effects of suction chamber geometry. Chem Eng Sci 2008;63:3886–97. https://doi.org/10.1016/j.ces.2008.04.012.
[19] Winoto SH, Li H, Shah DA. Efficiency of jet pumps. J Hydraul Eng 2000;126:150–6.
[20] Sanger NL. Noncavitating and Cavitating Performance of Two Low-area-ratio Water Jet Pumps with Throat Lengths of 5.66 Diameters. 1968. Nasa Tec Note.
[21] El Gazzar M, Meakhail T, Mikhail S. Numerical and experimental study of the influence of drag reduction agent (carboxy methyl cellulose) on the central jet pump performance. Proc Inst Mech Eng Part A J Power Energy 2007;221:1067–73. https://doi.org/10.1243/09576509JPE349.
[22] Pianthong K, Seehanam W, Behnia M, Sriveerakul T, Aphornratana S. Investigation and improvement of ejector refrigeration system using computational fluid dynamics technique. Energy Convers Manag 2007;48:2556–64. https://doi.org/10.1016/j.enconman.2007.03.021.
[23] Launder BE, Spalding DB. The numerical computation of turbulent flows. Comput Methods Appl Mech Eng 1974;3:269–89. https://doi.org/10.1016/0045-7825(74)90029-2.
[24] Wilcox DC. Turbulence modeling for CFD. 1993.
[25] Menter FR, Kuntz M, Langtry R. Ten years of industrial experience with the SST turbulence model F. Turbul Heat Mass Transf 2003;4:625–32.
[26] COMSOL Multiphysics. Introduction to COMSOL Multiphysics - user's guide. 2017.
[27] Ramesh AS, Joseph Sekhar S. Experimental studies on the effect of suction chamber angle on the entrainment of passive fluid in a steam ejector. J Fluids Eng Trans ASME 2018;140:1–8. https://doi.org/10.1115/1.4037692.
[28] Pope SB. Turbulent flows. Cambridge University Press; 2001.
[29] White FM. Viscous fluid flow. second ed. 1991.